Micro- and nano-structural evolutions in white Portland cement/pulverized fuel ash cement pastes due to deionized-water leaching

Shanshan Jia, Ian G. Richardson*

School of Civil Engineering, University of Leeds, Leeds LS2 9JT, United Kingdom

ARTICLE INFO

ABSTRACT

Thin slices of white Portland cement-low calcium pulverized fuel ash (pfa) blended cement pastes containing 30 or 50% pfa were leached progressively in de-ionized water. The paste with 50% pfa was aged 13 years prior to leaching and those with 30% pfa were aged 1 and 13 years. Pastes were leached for up to 75 days and were characterized using thermal analysis, X-ray diffraction, analytical scanning and transmission electron microscopy, and solid-state nuclear magnetic resonance spectroscopy. Leaching affected the pastes in the following sequence: (i) crystals of $Ca(OH)_2$ large enough to be resolved by backscattered electron imaging were removed completely prior to any effect on C-A-S-H; (ii) the Ca/Si ratio of C-A-S-H reduced from ≈ 1.4 to ≈ 1.0 whilst the aluminosilicate structure was unaffected; (iii) further reduction in the Ca/Si ratio of C-A-S-H was accompanied by lengthening of the aluminosilicate chains; (iv) the Ca/Si ratio of C-A-S-H reduced ultimately to ≈ 0.6.

1. Introduction

Cementitious materials will be used in a wide range of applications in the geological disposal facility (GDF) for radioactive waste in the UK. These include: waste encapsulation grouts, concrete waste containers, vault/tunnel backfills, lining and plugs; fracture grouts; and floors and roads [1–4]. Hardened cements are porous materials that contain a pore solution that is highly alkaline, with an initial pH that may be as high as ≈ 13 [5].

There are great advantages of utilising cementitious materials as waste encapsulation grouts for the packaging of intermediate-level wastes (ILW), e.g.; an alkaline chemistry ensuring low solubility for many radionuclides; immobilization of radionuclides because the structure can accommodate foreign ions; cost –effectiveness; and ready availability [6]. The long-term ability of a cementitious backfill to maintain an alkaline environment and take up radionuclides from solution are important contributors to the containment of radionuclides in ILW after the closure of a GDF [7].

Formulations of blends of ordinary Portland cement (oPc) with ground granulated blast-furnace slag (ggbs) or pulverized fuel ash (pfa) are commonly used in the UK for the packaging of ILW [8]. In this work, white Portland cement (wPc) was blended with pfa. wPc was used instead of oPc, because the lower quantities of paramagnetic ions (e.g. Fe^{3+}) result in narrower peaks in the solid-state nuclear magnetic resonance (NMR) spectra [9]. Richardson et al. compared the data from [10–12] and concluded that the morphology of the outer product (Op)

calcium aluminosilicate hydrate (C-A-S-H) in the hydrated cement is associated with a change of pH of the pore solution that occurs as the pfa reacts, the degree of saturation with respect to CH, and the Si concentration [13].

The cementitious materials will be leached by, and react with solutes in, groundwater moving through the vaults after closure of a GDF [14]. When these are leached by a groundwater with a low mineral content and approximately neutral pH, the main cement hydrate phases (e.g. first calcium hydroxide (CH) and later also C-A-S-H, AFt and AFm phases) will be dissolved or diffused out due to the concentration gradient between the pore solution of the cement and the surrounding groundwater, leading to a decrease of the pH of the pore solution and in the long-term the degradation of the cement [15,16]. The decrease of the pH in the long term may influence the performance of the GDF by increasing the solubility of radionuclides which are immobilized by the cementitious materials [6]. As the CH plays an important role in buffering the pH of the pore solution, the determination of its dissolution kinetics is important. In an oPc paste blended with pfa, wherein the CH is largely consumed by the pozzolanic reaction, the pH of the pore solution is mainly buffered by the C-A-S-H. Therefore, the dissolution kinetics and leaching behaviour of C-A-S-H and C-S-H have been the focus of significant efforts [17–19]. The purpose of this paper is to improve understanding of how the CH and C-A-S-H in wPc/pfa are affected by leaching, and thus to contribute to the knowledge underpinning the long-term evolution of the GDF.

---

* Corresponding author.
E-mail address: i.g.richardson@leeds.ac.uk (I.G. Richardson).

Table 1
Bulk oxide compositions of raw materials. ND, not determined.

	13-years-old sample		1-year-old sample	
	WPC	PFA (demagnetised)	WPC	PFA
SiO_2	25.00	51.80	24.81	50.41
TiO_2	0.08	1.00	ND	ND
Al_2O_3	2.14	26.14	2.35	24.10
Fe_2O_3	0.36	5.93	0.49	10.63
Mn_3O_4	0.02	0.06	ND	ND
MgO	0.78	1.59	0.80	1.60
CaO	71.02	1.67	70.64	3.40
Na_2O	< 0.30	1.48	0.15	0.89
K_2O	0.09	3.79	0.06	2.97
P_2O_5	0.08	0.24	ND	ND
Cr_2O	< 0.01	0.02	ND	ND
SO_3	ND	ND	2.03	0.48
Total	99.57	93.69	101.3	94.48
LOI at 1025 °C	1.06	3.40	< 0.01	ND

2. Experimental materials and techniques

Three sets of white Portland cement/pulverized fly ash (wPc/pfa) blended cement paste were used in the leaching experiments, i.e. one-year-old paste of 70 wt% wPc-30% pfa (1Y-WP30), 13-years-old paste of 70% wPc-30% pfa (13Y-WP30) and 13-years-old paste of 50% wPc-50% pfa (13Y-WP50). The 13-years-old cement paste was made by blending wPc (Aalborg, Denmark) with either 30% or 50% Class F pfa (National Powder, West Burton, U.K.) at a water/solid ratio of 0.50(mL/g). The resolution of the NMR spectra was improved by the removal of magnetic particles using the method described in [13]. The paste was cast in 5 mL polypropylene vials, sealed and cured at 25 ± 1 °C in a water bath for four years, then collected and stored in a desiccator. The 1-year-old wPc/pfa blended cement paste with 70% of wPc (Ribble wPc 8108, Castle Cement Limited, U.K.) and 30% of Class F pfa (Drax Power station, Selby, U.K.) was cast with the water/solid ratio of 0.50 (mL/g), and the paste was then cured in a water bath at 25 ± 1 °C. The bulk oxide compositions of wPc and pfa used in the study are shown in Table 1.

The paste was cut into 600 μm thick slices with a slow-speed diamond saw, placed on a stainless steel supporting frame, and then submerged into a sealed and continuously stirred water bath containing deionized water (liquid/paste mass ratio = 200), kept at room temperature (25 ± 1 °C). A photograph of the samples and supporting frame is shown in Fig. 1. Every five days, slices were collected and

Fig. 1. The apparatus for leaching experiments.

stored in a vacuum desiccator for later characterization. The leachate was replaced by fresh deionized water each time. The leaching experiments of the 1Y-WP30 13Y-WP30 and 13Y-WP50 cement paste took 75 days, 45 days and 55 days, respectively. Due to the limited amount of the 13-years-old pastes, the leaching experiment performed on those two samples was not continued for as long as for the one-year-old paste. This study involved multi-technique microstructural characterization, including use of simultaneous thermal analysis (STA), powder X-ray diffraction (XRD), scanning electron microscopy (SEM) with energy-dispersive X-ray analysis (EDX), transmission electron microscopy (TEM) with EDX, and solid-state ^{29}Si and ^{27}Al magic-angle spinning (MAS) NMR. Whilst such an approach has obvious benefits, in that the results from the different techniques provide complementary information, it is nevertheless important to recognize that there are limitations to the complementarity for inhomogeneous samples. The limitations stem from the fact that whilst the XRD, NMR and STA are bulk techniques that provide average information for a sample, the electron microscopy techniques provide microstructural and microchemical data that are specific to a particular location; this is discussed further below and in Section 3.

Thermal analysis was performed using a Stanton Redcroft STA 1000 (U.K.) equipped with simultaneous thermogravimetric (TG) and differential thermal analysis (DTA). Before loading, the sample was crushed and ground to fine powder in an agate mortar. The sample was loaded in a platinum crucible and was heated up to 1000 °C from 25 °C at a rate of 20 °C/min, under a constant flow of nitrogen gas (BOC, U.K.) at 58 mL/min. The amount of CH present in the sample was calculated from the TG curve using the 'tangent' analysis method to exclude mass loss due the concurrent dehydration of other phases [20].

The XRD measurements were performed using a Panalytical X'PERT-PRO diffractometer system (with X'Celerator real time multiple strip detector), operated with Cu kα radiation at 40 mA and 45 kV. Before loading the sample, the paste was crushed and ground into fine powder in an agate mortar. The powder sample was mounted on a holder that was spun at 2 revolutions per second and the XRD pattern acquired in continuous scan mode over the range of 5 to 80° 2θ with a step size of 0.0334° 2θ (i.e. 2244 steps), leading the total acquisition time of about 1 h.

Samples for examination by SEM were prepared as follows: The slice of cement paste that had been dried in the vacuum desiccator was impregnated with epoxy-resin (Epofix Kit, Struers, UK) under vacuum and allowed to set for 1 day; it was demoulded and polished to a flat surface using a polishing/grinding machine (PdM-Force20 mounted on Struers Rotopol-35) using silicon carbide paper of two different grades (500 μm and 1200 μm grit) and subsequently with diamond paste cloth of 6, 3, 1, and ¼ μm (Struers, U.K.); the polished surface was then carbon coated in an EMSCOPE TB500 (U.K.) vacuum coating machine with a thickness of 15 nm to avoid charging during SEM examination. The SEM examinations were performed on a Carl Zeiss EVO MA15 variable pressure W SEM with Oxford Instruments INCA EDX system with a 80 mm X-Max SDD detector. The modes used in the study were backscattered electron imaging, EDX elemental mapping and EDX point analysis. The microscope was operated at an accelerating voltage of 20 kV, with a working distance of 8 mm and a spot size of 5. The magnification used in the study was 500 ×. The sample preparation procedure generally removed about 60 to 100 μm from the surface of each section – although sometimes less – and so most EDX analyses correspond to this approximate depth (an example is given in Section 3.2). However, four specimens of 1Y-WP30 were sectioned perpendicular to the leached surface, thus enabling measurement of a Ca/Si ratio depth profile for different leaching times (0, 15, 45 and 75 days); this was not possible for the 13-year-old samples because of the limited quantity available. Samples for examination by TEM were prepared as follows: (i) The slice of cement paste was thinned by hand using 1200 grit silicon carbide paper to get a flat surface, which removed approximately 35 μm of the section; (ii) the flat surface was glued to a
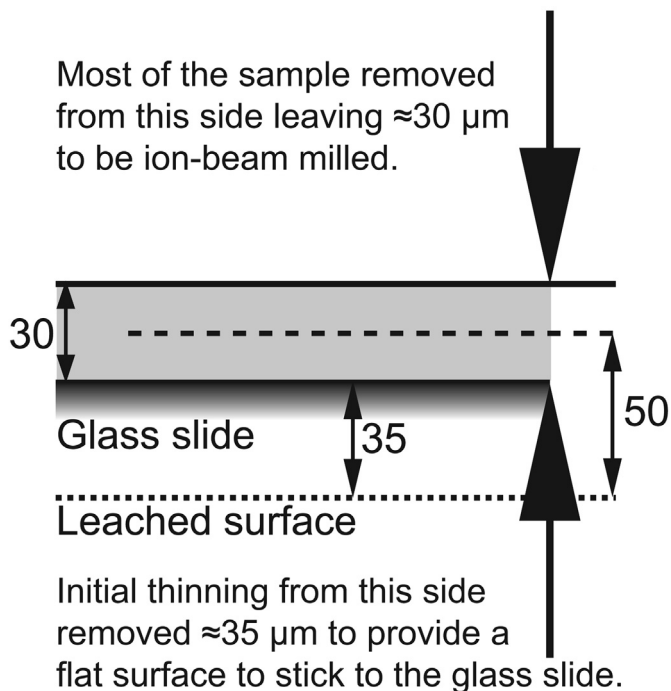
Most of the sample removed from this side leaving ≈30 μm to be ion-beam milled.

30

Glass slide 35

50

Leached surface

Initial thinning from this side removed ≈35 μm to provide a flat surface to stick to the glass slide.

Fig. 2. Schematic illustration of the TEM sample preparation procedure. The distances are approximate i.e. the figure shows the TEM specimen corresponding to a depth into the cement disk of 50 μm although in practice it probably varied between 20–60 μm.

glass slide; (iii) polishing was continued using 1200 and 2400 grit silicon carbide paper until the sample was approximately 30 μm thick; (iv) the glue was dissolved using acetone and the sample 'sandwiched' between copper grids with a 3×1 mm hole in the middle; (v) the sample was argon ion-beam milled (Model 1010 Ion Mill, Fischione Instruments, PA, U.S.A.) using a liquid nitrogen cooled stage to avoid specimen heating and consequent damage. The milling was performed until a small hole was visible at the centre of the sample, which took around 10–30 h depending on the nature of the sample. The TEM sample preparation procedure is illustrated in Fig. 2; it is evident that the TEM specimens that were examined in this study corresponded to an approximate depth into the cement disks of 50 μm, although in practice it probably varied between 20–60 μm. Each TEM specimen was carbon coated using an Agar Turbo Carbon Coater equipped with an Agar thickness monitor and stored in a desiccator prior to TEM examination to avoid carbonation. The TEM examinations were performed on a FEI Tecnai TF20 TEM equipped with Oxford Instruments INCA EDX system for nano-scale imaging and EDX analysis. Before acquiring each EDX analysis, areas ostensibly of C-A-S-H were checked for intermixing with crystalline phases using selected area electron diffraction (SAED). The EDX analyses were taken randomly in the thin area of the sample, at magnification of $17,500 \times$ and spot size 8; analysis areas were kept at around 200 nm in diameter because a more finely focussed electron beam causes spurious results due to beam damage [21].

The solid-state ^{29}Si MAS NMR measurements were performed on a Varian InfinityPlus 300 spectrometer (magnetic field 7.0 T; operating frequency 59.5 MHz) equipped with Chemagnetics style MAS probes. Before loading, the vacuum dried paste was ground into fine powder in an agate mortar and evenly packed in a 6-mm diameter zirconia rotor sealed with Teflon end caps. The ^{29}Si MAS NMR spectra were acquired using a spinning speed of 7 kHz, pulse recycle delay of 5 s, pulse width of 5 μs and acquisition time of 20 ms, with over 10,000 scans. The ^{27}Al MAS NMR measurements were performed on a Varian VNMRS spectrometer (magnet field 9.4 T; operating frequency 104.198 MHz) equipped with 4 mm pencil MAS probes. The spectra were acquired

Table 2
Phases observed by XRD in the unleached 1Y-WP30, 13Y-WP30 and 13Y-WP50 cement pastes and after 45 days and 75 days of leaching.

		C-A-S-H	CH	Belite	AFt	AFm	Quartz	mullite
Before leaching	1Y-WP30	✓	✓	✓	✓	✗	✓	✓
	13Y-WP30	✓	✓	✓	✓	✗	✓	✓
	13Y-WP50	✓	✗	✓	✓	✗	✓	✓
After leaching	1Y-WP30 (45 day)	✓	✗	✓	✓	✗	✓	✓
	1Y-WP30 (75 day)	✓	✗	✗	✗	✗	✓	✓
	13Y-WP30 (45 days)	✓	✗	✓	✓	✗	✓	✓
	13Y-WP50 (45 days)	✓	✗	✓	✓	✗	✓	✓

using a spinning speed of 14 kHz, pulse recycle delay of 0.2 s, pulse width of 1 μs and acquisition time of 10 ms, with over 7000 scans.

3. Results and discussion

3.1. Phase identification and quantification studied by XRD and thermal analysis

The phases observed by XRD in the 1Y-WP30, 13Y-WP30 and 13Y-WP50 cement pastes before and after leaching are indicated in Table 2. The crystalline phases in the unleached cement paste included some residual belite, quartz and mullite from the fly ash [22,23], AFt and CH, which was the most abundant crystalline phase. The main hydration product, C-A-S-H, is indicated on the diffraction pattern for the unleached cement paste by diffuse peaks at about 3.0 and 1.82 Å. Whilst some residual belite would be expected to be present in a neat white cement paste after 1 year hydration at ordinary temperatures (e.g. [24]), the hydration of belite has also been reported to be retarded by the presence of fly ash particles (e.g. [25]). An AFm phase was not observed by XRD but a peak assigned to it is present on the ^{27}Al NMR spectrum (see Section 3.4), which indicates that any AFm was at best poorly crystalline, perhaps due to the opposite charges on the main layers in the structures of AFm and C-A-S-H producing strong mutual attraction that results in interstratification and loss of long-range order [26].

The XRD results show that after 45 days of leaching (i.e. after 9 replacements of deionized water) the CH had been dissolved completely from all three types of cement pastes and the content of belite had also decreased. CH with $K_{SP} = 6.5 \times 10^{-6}$ at 25 °C [27] is easily dissolved by water and the decrease in the belite content was likely to be due to secondary hydration because of the additional water [28]. AFt was still detectable by XRD in all three of the cement pastes after 45 days of leaching, however, it was absent after 75 days. The absence of AFt is confirmed by the absence of a peak at ≈ 13 ppm on the ^{27}Al NMR spectrum (see Section 3.4).

Fig. 3 shows how the total CH content determined by TG varied during the leaching process for the three cement pastes. Before leaching, the 1Y-WP30 cement paste had the most CH (13.9%), followed by the 13Y-WP30 paste (10.6%) and finally the 13Y-WP50 had the least (6.3%) because of the lower amount of white cement in the paste and the greater consumption of CH by the pozzolanic reaction. The CH in all three pastes had been dissolved completely by 45 days of leaching. The CH dissolution trend is largely consistent with that observed by Girão [29], who also studied the leaching of 1-year-old wPc-30% pfa blends using a very similar experimental arrangement: Girão found that the CH had dissolved by 4 weeks of leaching rather than the 5 weeks reported here, followed by the short-term reappearance of CH, which was attributed to the hydration of residual belite.
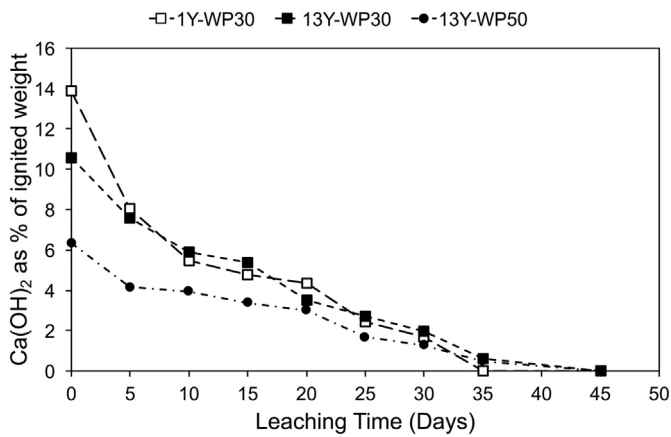
Fig. 3. The CH as a percentage of ignited weight determined by TG at different leaching time in the 1Y-WP30, 13Y-WP30 and 13Y-WP50 cement pastes.

3.2. Evolution of structure and chemical composition at micro-scale studied by SEM-EDX

The microstructure of the unleached 1Y-WP30 cement paste included unhydrated cement and pfa particles, CH, C-A-S-H and porosity, as illustrated in Fig. 4(a), which is a typical BSE image taken at 500 × magnification; this is in agreement with the observations of Girão [29] and Love [30] who both studied similar pastes. The CH is abundant in the micrograph, which is consistent with the XRD and thermal analysis observations, and anhydrous wPc grains are also present. In the unleached 1Y-WP30 cement paste, the mean Ca/Si ratio of the analyses that were identified microstructurally as likely to be C-A-S-H was 1.42 ± 0.09 ($n = 38$); however, caution should be taken when interpreting the results of SEM-EDX analyses of hardened cement pastes because hydration products are commonly intermixed at a scale that is much finer than the X-ray generation volume [21], which is discussed further below. Regions believed to be predominantly C-A-S-H were identified by microstructure and grey-scale and the corresponding EDX analyses include both Ip and Op C-A-S-H. Fig. 4(b) is a BSE image of a region in the degraded layer of the 1Y-WP30 cement paste after 15 days

of leaching. It shows that there was little CH left in that particular area and greater porosity when compared to the unleached 1Y-WP30 sample. An equivalent micrograph for the paste after 45 days of leaching is shown in Fig. 4(c). In this case, there is no CH evident, and the wPc grains are fully hydrated. Fig. 4(d) shows a representative BSE image of the degraded layer of the 1Y-WP30 cement paste after 75 days of leaching (in this case, the microstructure is entirely zone 4, as defined below), which demonstrates the general dry cracked land-like microstructure (the large cracks are filled with resin). Cracks in cementitious material generally interconnect flow paths and increase permeability [31]. A large amount of unreacted pfa was still evident in the leached paste, especially those pfa particles that were iron-rich (as analysed by EDX).

Fig. 5 presents typical BSE images of the unleached 13Y-WP30 and 13Y-WP50 cement pastes ((a) and (c)) and after 45 days of leaching ((b) and (d)). The main phases in the sample with 30% pfa before leaching (Fig. 5(a)) are the same as those of the one-year-old sample (Fig. 4(a)), i.e. wPc grains, pfa, CH and C-A-S-H. However, the microstructure is more homogeneous and compact due to further cement hydration [32]. Regions of CH are still evident in the micrographs for 13-years-old samples, which is consistent with the presence of the CH in the TG and XRD results (Section 3.1). It is evident on comparison of micrographs for these two sets of blended cement pastes that there are more pfa particles in 13Y-WP50 than in 13Y-WP30, as expected given the higher pfa content and lower amount of CH available for reaction. Fig. 5(b) and (d) show examples of the microstructures of the degraded layers of the 13-years-old samples after 45 days of leaching. The microstructures have changed significantly with a clear increase in porosity.

Fig. 6 presents the average Ca/Si atom ratio of analyses seemingly of the C-A-S-H present in the unleached 1Y-WP30, 13Y-WP30 and 13Y-WP50 cement pastes and from the degraded layer of the pastes after different periods of leaching. As stated in Section 2, due to the nature of the SEM sample preparation, the EDX analysis was performed approximately 60 to 100 μm from the surface of each sample. Before leaching, the average value in the 1Y-WP30 and 13Y-WP30 cement pastes is close, i.e. $Ca/Si = 1.42 \pm 0.09$ ($n = 38$) and 1.43 ± 0.04 ($n = 30$) respectively, which are statistically significantly higher than that in the paste with 50% pfa (with $Ca/Si = 1.32 \pm 0.09$ ($n = 22$)). The figure shows that during the first 5 days of leaching, the C-A-S-H at
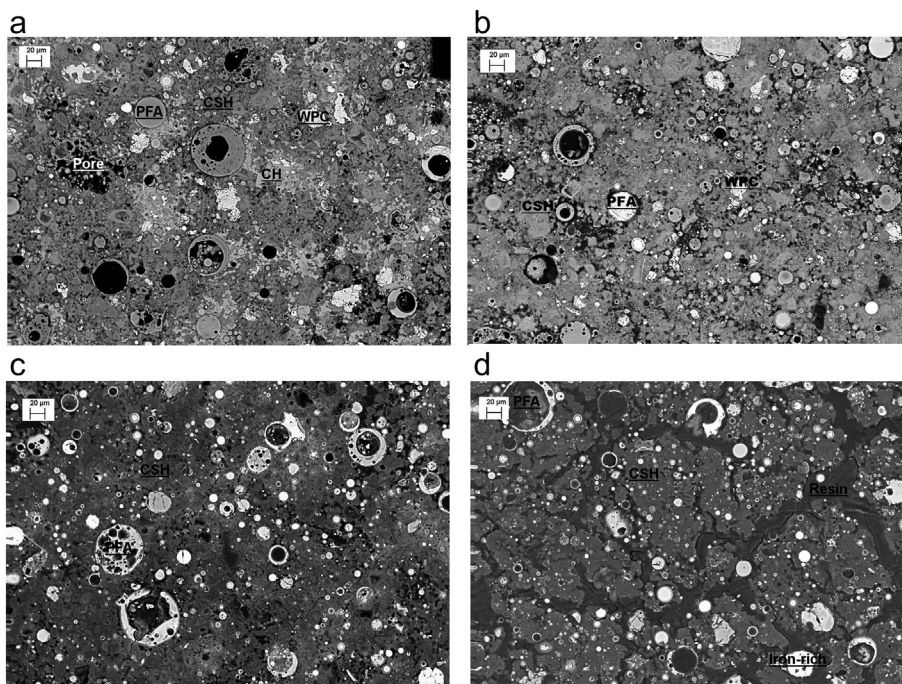

Fig. 4. BSE images illustrating the microstructure of (a) the unleached 1Y-WP30 cement paste, and after leaching times of (b) 15 days, (c) 45 days, and (d) 75 days. Regions of pulverized fly ash (PFA), white Portland cement (WPC), calcium hydroxide (CH), C-A-S-H (CSH) and pores (Pore) are labelled.
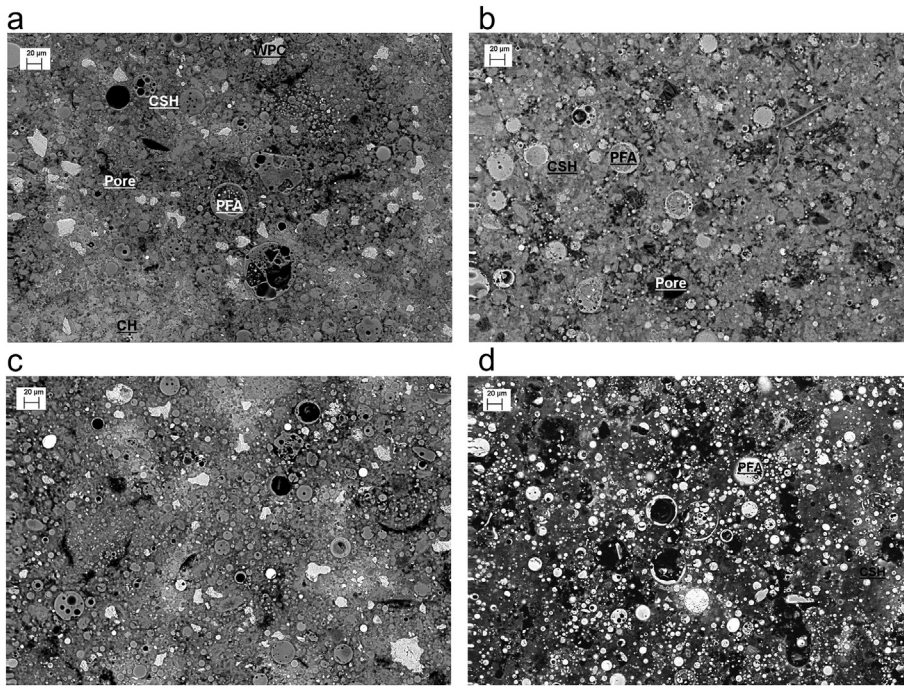
Fig. 5. BSE images illustrating the microstructures of the unleached 13Y-WP30 and 13Y-WP50 cement pastes (Fig. (a) and (c) respectively), and after 45 days of leaching ((b) and (d)). Regions of pulverized fly ash (PFA), white Portland cement (WPC), calcium hydroxide (CH), C-A-S-H (CSH) and pores (Pore) are labelled.
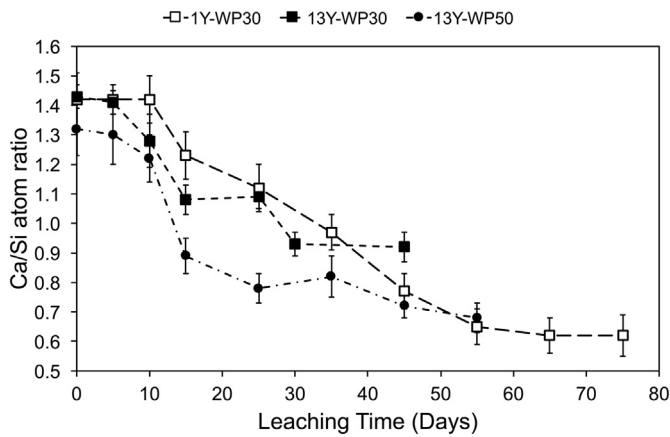

Fig. 6. Average Ca/Si atom ratios for the 1Y-WP30, 13Y-WP30 and 13Y-WP50 cement pastes observed by SEM-EDX phase analysis of C-A-S-H as a function of leaching time.

the sampled depth in all three pastes was essentially unaffected by the leaching. Since the CH contents of the whole disks were much reduced at 5 days, this suggests that the CH had started to be dissolved before the C-A-S-H was affected. By 10 days of leaching, the C-A-S-H in the 13Y-WP30 and 13Y-WP50 cement pastes had started to be decalcified, whilst it was still unaffected in the 1Y-WP30 cement paste, possibly due to the larger amount of CH present initially in the 1-year-old sample, which postpones decalcification of the C-A-S-H. The C-A-S-H at the sampled depth in all the pastes leached for 15 days had experienced significant decalcification, as at this stage the CH had been dissolved thoroughly at this depth, as observed by SEM imaging. Longer leaching times resulted in only modest further reduction in the Ca/Si ratio for the 13-year-old samples, although it was not possible to evaluate whether it had already reached the C-A-S-H decalcification limit due to the limited amount of those samples available, which was insufficient to extend the experiments beyond 45 days of leaching. In contrast, the leaching experiment was continued for a much longer period for the 1Y-WP30 cement paste: after 55 days of leaching, the Ca/Si ratio had decreased to 0.65 ± 0.06 ($n = 40$). Afterwards, the Ca/Si atom ratio did not change significantly, and after 75 days of leaching it was

0.62 ± 0.07 ($n = 33$), suggesting that the C-A-S-H decalcification was approaching a constant value, consistent with work on the leaching of synthetic C-S-H using demineralised water [33].

As noted, the results reported in Fig. 6 correspond to a sampling depth of ≈ 60–100 μm. In contrast, Fig. 7 shows Ca/Si ratios measured at different depths by SEM-EDX for the 'C-A-S-H' present in the 1Y-WP30 paste leached for 0, 15, 45 and 75 days. Unsurprisingly, the Ca/Si ratio in the unleached paste (△) is essentially constant throughout the thickness of the section, matching the value reported above that was determined using a section cut parallel to the face of the disk. The profile for the sample that had spent 15 days in the water bath (○) reveals clearly the effects of leaching on the C-A-S-H: The Ca/Si ratio at the surface had been reduced to about 0.93; it then increases linearly with distance into the disk, reaching the same value as the unleached paste at a depth of about 170 μm. 45 days in the water bath (●) resulted in a further decrease in the Ca/Si at the surface to about 0.63; again, it then increases linearly with distance into the disk, reaching the same value as the unleached paste at a depth of about 270 μm. It is notable that the gradient in the Ca/Si ratio was essentially the same at 45 days as at 15 days, with the Ca/Si ratio in both cases reducing from the
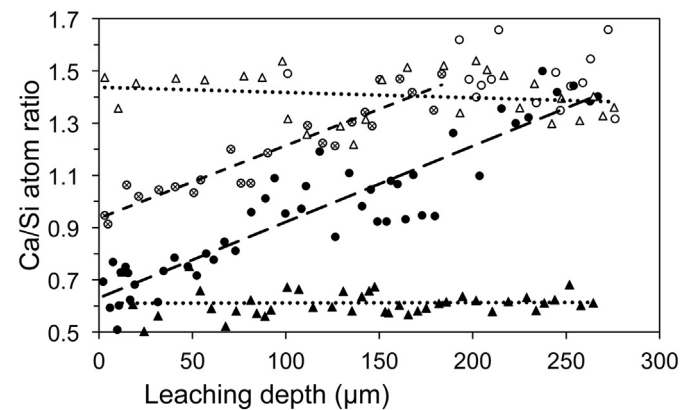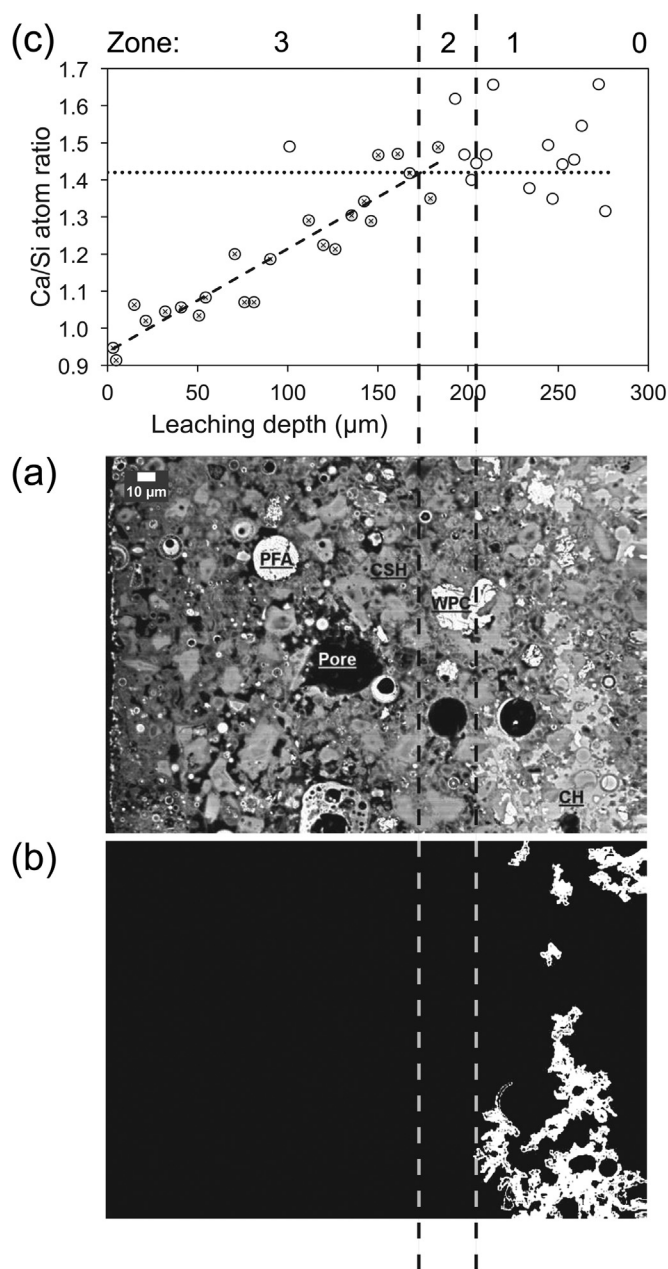

Fig. 7. Ca/Si ratio profiles measured by SEM-EDX for the C-A-S-H present in the 1Y-WP30 paste leached for 0 (△), 15 (○), 45 (●) and 75 days (▲). Each data point is from a single EDX analysis of an area that appeared microstructurally to be C-A-S-H. Data points used for the regression analysis are indicated using a ×.

Fig. 8. SEM-EDX analysis results for a cross-section of the 1Y-WP30 cement paste after 15 days of leaching, including: (a) a BSE image of the region where the surface exposed to water is on the left-hand side (regions of white Portland cement (WPC), pulverized fly ash (PFA) and C-A-S-H (CSH) are labelled); (b) a binary mask that shows areas of calcium hydroxide in the image; and (c) a plot of the Ca/Si ratio of the C-A-S-H against leaching depth. Data points used for the regression analysis are indicated using a ×.

unleached value of 1.43 by $\approx 0.3/100\,\mu m$. No further significant reduction was observed in the Ca/Si ratio at the surface with additional time in the water bath; the Ca/Si ratio profile appears to have simply progressed through the thickness of the disk until there was a constant value of about 0.61, as shown in Fig. 7 for 75 days (▲). It is thus evident that increasingly longer times in the water bath resulted in a Ca/Si ratio profile of essentially fixed gradient that moved through the thickness of the sample; the maximum width of this zone was about 270 μm.

Comparison of the data in Fig. 6 with the profiles in Fig. 7 suggests that the sampling depth at 15 days was quite deep ($\approx 100\,\mu m$), whereas at 45 days it was probably quite shallow ($\approx 50\,\mu m$).

The movement of this profile through the sample with progressive

leaching of calcium resulted in microstructural changes that are usefully categorized as 5 zones. Three of these zones are illustrated in Fig. 8, which includes a replot of the Ca/Si ratio profile for the 15-day sample from Fig. 7, together with the corresponding BSE image of the region (where the surface exposed to water is on the left-hand side) and a binary mask that shows large areas of calcium hydroxide in the image (derived using the greyscale histogram from the BSE image). The horizontal dotted line in Fig. 8(c) represents the mean Ca/Si ratio of the C-A-S-H in the unleached paste determined by SEM-EDX (using a sample that had been taken parallel to the surface), namely 1.42 (standard deviation = 0.09, number of analyses, $n = 38$). It is probable that this value was affected by intermixing of the C-A-S-H with other phases and that the true value for the C-A-S-H is slightly smaller, as observed previously by TEM-EDX for a similar system [13]. The short-dash line is the result of the linear regression fit to the data points that are marked with a cross: the equation is Ca/Si = 0.9358 + 0.0028(depth); $r^2 = 0.89$. As noted above, it is evident that starting from the value of the unleached C-A-S-H, the Ca/Si ratio reduces linearly with distance as the surface that is exposed to water is approached; the gradual leaching of calcium from the surface of the disks resulted in the five microstructural zones (0 to 4, in part illustrated in Fig. 8), which correspond to the following features:

Zone 0: Unleached.

Zone 1: A reduced quantity of $Ca(OH)_2$ but the C-A-S-H is unaffected.

Zone 2: No large crystals of $Ca(OH)_2$ and the C-A-S-H is unaffected.

Zone 3: No $Ca(OH)_2$ and the Ca/Si ratio of the C-A-S-H is lower than in the unleached paste; the Ca/Si ratio reduces linearly with distance from zone 2, reducing from the unleached value of 1.43 by $\approx 0.3/100\,\mu m$.

Zone 4: No $Ca(OH)_2$ and the Ca/Si ratio of the C-A-S-H reduced to about 0.6; this zone is only present after significant leaching.

With reference to these five zones, the following terms are defined that are used in the discussion:

(i) The '*degraded layer*' comprises zones 1 to 4 i.e. it is the part of the disk where there is evidence of microstructural alteration due to leaching;

(ii) the '*CH dissolution depth*' comprises zones 2 to 4 i.e. it is the distance into the disk where there are no longer any large crystals of $Ca(OH)_2$ present (i.e. crystals that are sufficiently large to be resolved by BSE imaging); and

(iii) the '*C-A-S-H decalcification depth*' corresponds to zones 3 and 4 i.e. it is the distance into the disk where a detectable quantity of calcium has been removed from the C-A-S-H.

For the 1Y-WP30 cement paste, the C-A-S-H decalcification depth was 170 μm after 15 days leaching and 270 μm after 45 days; the CH dissolution depth was 200 μm after 15 days and 300 μm after 45 days i.e. throughout the thickness of the slice, which is consistent with the absence of CH in the TG data for this paste, as shown on Fig. 3. Decalcification of C-A-S-H must occur after the dissolution of large CH crystals (because the decalcification depth is shallower than the CH dissolution depth), which agrees with previous experimental and modelling investigations of cement paste leaching [34,35].

Fig. 8 (a) is a typical BSE image of the cross section of the 1Y-WP30 cement paste after 15 days of leaching. The same zoning as observed for the 1-year-old paste was also observed for the 13-year-old sample, which is illustrated in Fig. 9. Fig. 9(a) is a plot of leaching time against the C-A-S-H decalcification depth (●) and the CH dissolution depth (■). The shading indicates the approximate depths of sampling for measurement of Ca/Si ratios for both TEM and SEM, the latter being generally slightly deeper. Fig. 8(c) shows that the Ca/Si ratio of the C-A-S-H in zone 3 of the 1-year-old paste reduced linearly with distance from the interior of the disk to the leached surface and there is no reason to suppose that the situation was any different for the 13-year-
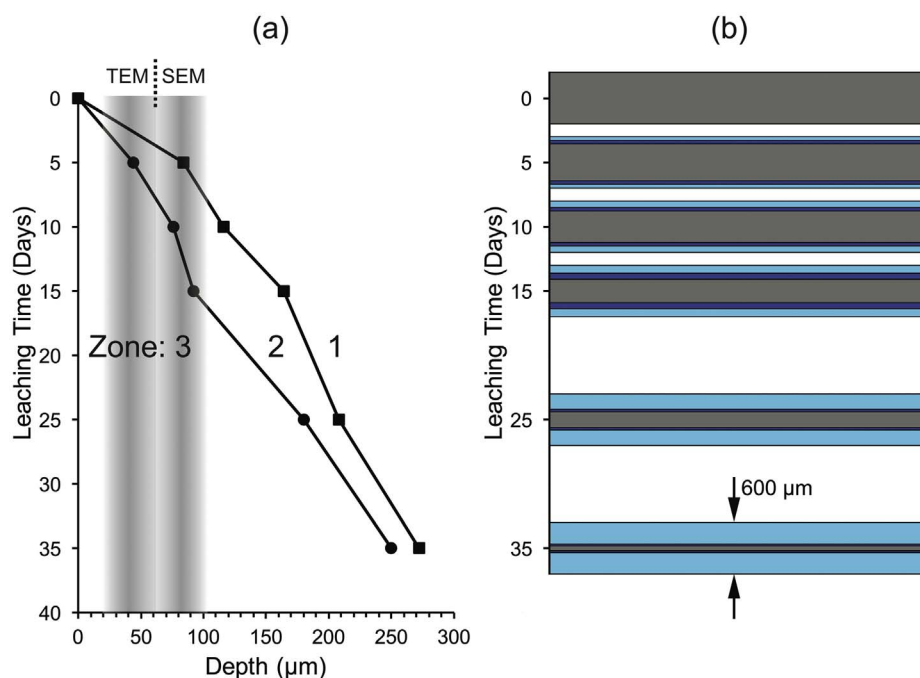
Fig. 9. (a) A plot of leaching time against the C-A-S-H decalcification depth (●) and the CH dissolution depth (■) for the sample 13Y-WP30. The shading indicates the approximate depths of sampling for measurement of Ca/Si ratios for both TEM and SEM, the latter being generally slightly deeper. (b) A schematic representation of cross sections through the central approximate third of the cement paste disks at each leaching time. Light blue = zone 3; dark blue = zone 2; grey = zones 1 and 0 (the microstructural zones are explained in Section 3.2). (For interpretation of the references to colour in this figure legend, the reader is referred to the web version of this article.)

Table 3

Mean Ca/Si and Al/Si ratios of the C-A-S-H present in the 13Y-WP30 samples as determined by TEM-EDX and the mean Ca/Si ratios for analyses nominally of C-A-S-H determined by SEM-EDX analysis. s.d. = standard deviation and *n* is the number of analyses. The error bars on the figure correspond to ± 1 s.d.

Leaching time (days)	TEM					SEM		
	n	Mean Ca/Si	s.d.	Mean Al/Si	s.d.	*n*	Mean Ca/Si	s.d.
0	48	1.37	0.11	0.19	0.03	30	1.43	0.04
5	39	1.32	0.12	0.20	0.03	41	1.41	0.04
10	37	1.10	0.07	0.20	0.02	25	1.28	0.09
15	48	1.04	0.09	0.20	0.05	41	1.08	0.05
25	48	0.95	0.08	0.22	0.05	28	1.09	0.04
35	38	0.85	0.09	0.24	0.03	35	0.93	0.04

old sample. Since the specimens used for TEM were closer to the surface than those for SEM (as discussed in Section 2 and as indicted in Fig. 9(a)), the values determined by TEM-EDX would be expected to be lower than those determined by SEM-EDX, which is indeed as was observed: the mean Ca/Si ratios, standard deviation and number of analyses are given in Table 3. Since the analysis in the TEM measures the composition of the C-A-S-H free of intermixture with other phases, the mean Ca/Si ratio of the C-A-S-H present in the unleached paste can be taken to be 1.37. The line on Fig. 9(a) that corresponds to the C-A-S-H decalcification depth (●) thus represents a compositional boundary: C-A-S-H to the right of this line would have mean Ca/Si = 1.37 (i.e. in zones 2, 1 and 0), and that to the left would have mean Ca/Si < 1.37. It is thus clear from inspection of Fig. 9(a) that at short leaching times, the Ca/Si ratios measured by SEM-EDX do not relate to a part of the sample where calcium has been leached from the C-A-S-H, i.e. zone 3; whilst the difference between the mean Ca/Si ratios given in Table 3 for 0 and 5 days is statistically significant, both values are > 1.37 and must correspond to zone 1 microstructure.

Fig. 9(b) is a schematic representation of cross sections through the central approximate third of the 13Y-WP30 cement paste disks at each leaching time (light blue = zone 3; dark blue = zone 2; grey = zones 1 and 0). It is very clearly evident from this figure why the results from the STA and NMR experiments – which are for whole disks, and thus represent average information – cannot generally be related directly to

the TEM-EDX and SEM-EDX microchemical data, which correspond to particular depths, as described above.

3.3. Evolution of structure and chemical composition as revealed by TEM-EDX

A typical TEM image of partially hydrated pfa from the 13Y-WP30 cement paste is shown in Fig. 10(a). Foil-like Ip C-A-S-H is present in the reacted pfa particle that is evidently lower density than the fine homogeneous product that is typical of Ip in reacted alite particles [36–38], which is illustrated in Fig. 10(b). The inner core of the pfa particle is surrounded by denser Op C-A-S-H. Many partially reacted pfa particles were observed in the 13-year-old sample. Fig. 11(a) illustrates the foil and net-like Op C-A-S-H from the degraded surface of the 13Y-WP30 cement paste after 45 days of leaching. The transformation from a mixed fine-fibrillar/foil-like morphology for Op C-A-S-H before leaching to a coarser foil and net-like morphology after leaching, is associated with the loss of Ca ions from the interlayer region of the C-A-S-H structure and lengthening of the aluminosilicate chains. Fig. 11(b) shows decalcified C-A-S-H intermixed with long, coarse fibre-like Op C-A-S-H, which was perhaps formed during the secondary hydration and coarser than usual because of the greater amount of space available for growth because of the leaching (the morphology of Op C-A-S-H depends on the space that is available for it to form [36,38]).

Fig. 12(a) is a typical micrograph for the unleached 13Y-WP50 sample, which shows examples of partially unreacted and glassy fly ash, fine fibrillar Op C-A-S-H, as well as foil-like Ip C-A-S-H formed in the pfa. A typical TEM image of the 13Y-WP50 cement paste after 55 days of leaching is presented in Fig. 12(b), which includes a number of fully hydrated pfa grains. Such features are not common in unleached pastes, which suggests that water leaching had induced further hydration of the pfa. It also illustrates the variable morphology of Ip C-A-S-H in hydrated pfa, which is not easily done with unleached pastes because the degree of hydration is generally not sufficient. The different morphologies are possibly caused by variations in the chemical composition and reactivity of glassy pfa; as Diamond pointed out, pfa particles within the same type of pfa can have different compositions [39]. The Ip C-A-S-H in the hydrated pfa particle labelled 1 on Fig. 12(b) has a fine, homogeneous morphology that is similar to that formed in neat Portland cement pastes, whilst it is less homogeneous in particle 2.
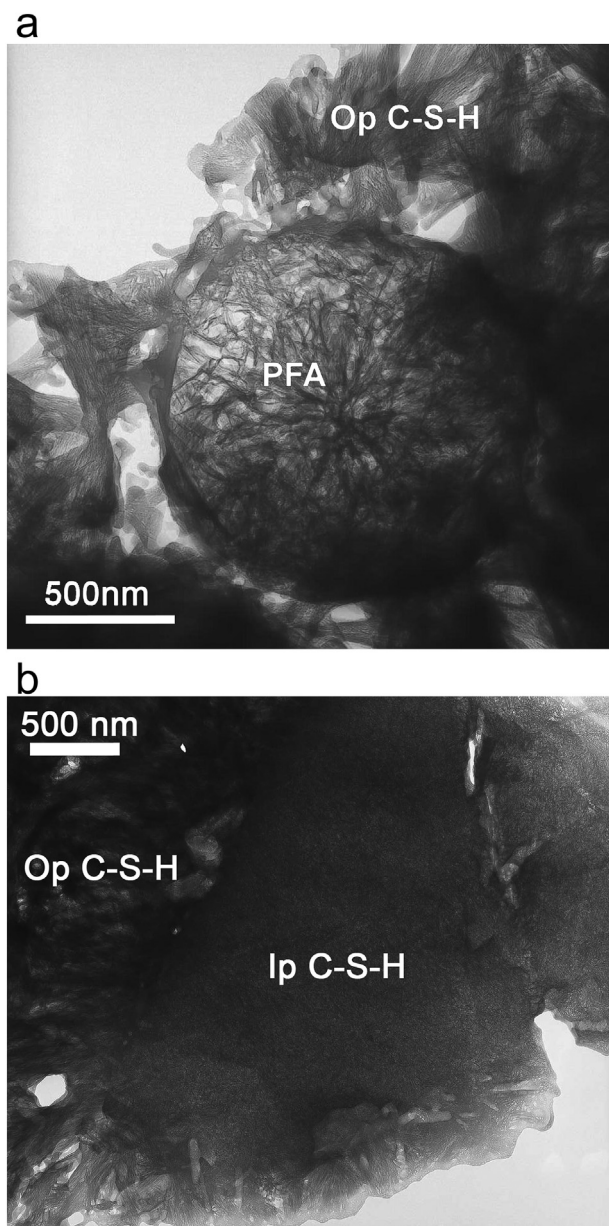
a

b

Fig. 10. TEM images from the unleached 13Y-WP30 cement paste showing: (a) partially hydrated pfa with low density foil-like Ip C-A-S-H and fine fibrillar Op C-A-S-H; (b) hydrated wPc with compact and homogeneous Ip C-A-S-H and fine fibrillar Op C-A-S-H.

a

b

Fig. 11. TEM images from the 13Y-WP30 cement paste after 45 days of leaching illustrating (a) foil and net-like decalcified Op C-A-S-H; and (b) decalcified short C-A-S-H intermixed with long coarse fibrillar Op C-A-S-H.

Other phases are intermixed with the C-A-S-H in particles 3 to 5; in particular, the needle-like features that are prominent in particle 3 analysed as being high in Mg and Al, and so can be identified as a hydrotalcite-like phase.

The results of TEM-EDX analyses of Ip and Op C-A-S-H in the unleached 13Y-WP30 cement paste are plotted on a CaO-Al_2O_3-SiO_2 ternary diagram in Fig. 13(a). The diagram clearly shows that the Ca/Si atom ratio of Ip and Op C-A-S-H is similar; the mean value for all analyses of C-A-S-H is 1.37 ± 0.11 (n = 48), Table 3. Mean values ranging between 1.32 and 1.38 were obtained for samples of the same paste at 1, 4, 9 and 13 years old [13,32], with some statistically significant differences that do not correspond to advancing age. Since the % CH was observed to reduce with time, indicating increased hydration of the pfa, the conclusion must be that there is some real variability within individual samples that results in sampling error between TEM specimens, although the differences are smaller than those between companion TEM-EDX and SEM-EDX analyses. The Ca/Si atom ratio
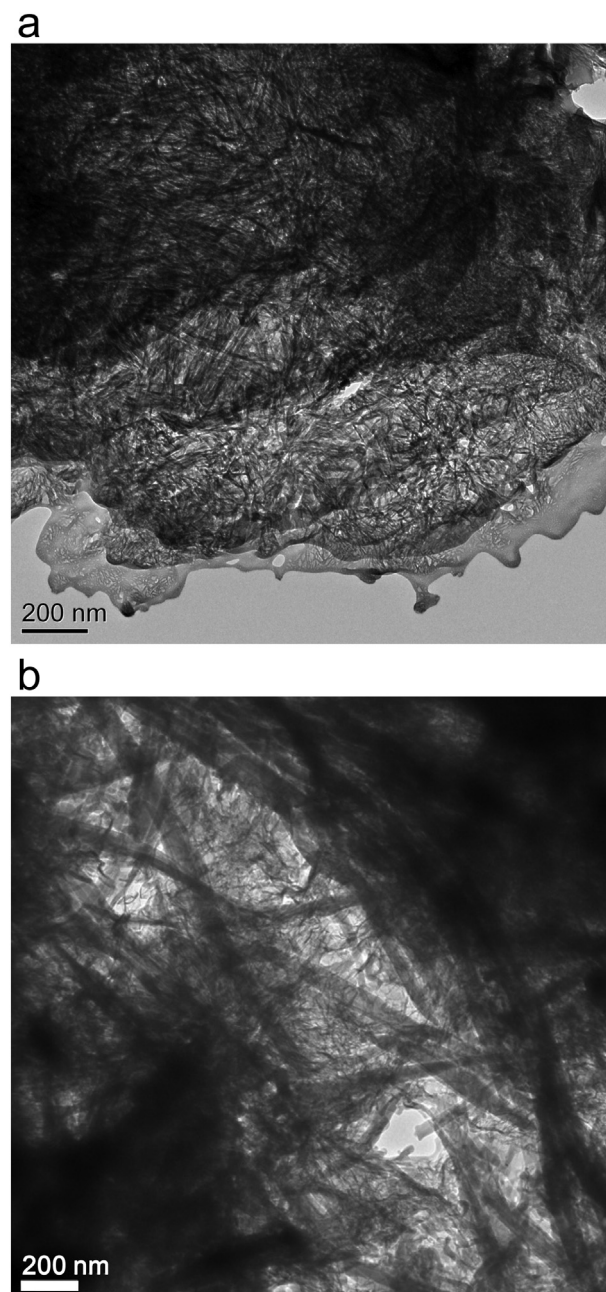
observed by TEM-EDX is slightly lower than that observed by SEM-EDX because the SEM-EDX has a larger X-ray generation volume, resulting in analyses of C-A-S-H intermixed with other phases. The TEM-EDX analyses of Ip and Op C-A-S-H on the degraded surface of the 13Y-WP30 cement paste after 45 days of leaching are plotted on a CaO-Al_2O_3-SiO_2 ternary diagram in Fig. 13(b). It is evident that the points are more scattered than those for the unleached sample, indicating that the C-A-S-H is more inhomogeneous.

Fig. 14(a) shows the CaO-Al_2O_3-SiO_2 ternary diagram of the C-A-S-H in the unleached 13-WP50 cement paste. The diagram indicates that the presence of the intermixture of CH with C-A-S-H, as there is a trend line in the direction of CH. As for the paste with 30% pfa, the average Ca/Si atom ratio measured by TEM-EDX (1.26 ± 0.12; n = 25) is significantly lower than that analysed by SEM-EDX (1.32 ± 0.09, n = 36), presumably for the same reason. TEM-EDX analyses of the C-
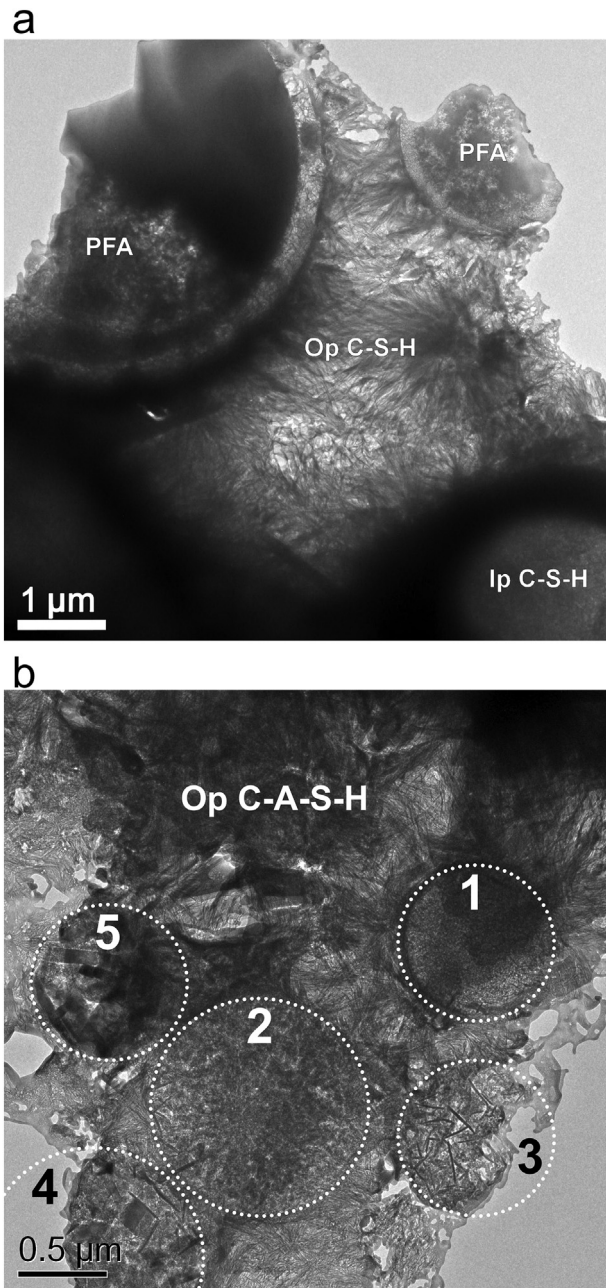
Fig. 12. TEM images of (a) the unleached 13Y-WP50 cement paste showing partially hydrated fly ash grains, fine fibrillar Op C-A-S-H, and foil-like Ip C-A-S-H; and (b) the degraded surface of the 13Y-WP50 cement paste after 55 days of leaching illustrating the variable morphology of fully hydrated pfa grains, which are indicated with white-dotted circles.

Fig. 13. CaO-Al$_2$O$_3$-SiO$_2$ ternary diagrams for TEM-EDX phase analysis of the C-A-S-H in the 13Y-WP30 cement paste before leaching (a) and after 45 days of leaching (b).

A-S-H in the 13-WP50 cement paste after 55 days of leaching are shown in Fig. 14(b). Comparison with Fig. 14(a) shows that the Ca/Si ratio decreased dramatically upon leaching; the mean value is 0.68 ± 0.05 (n = 45).

3.4. Evolution of nanostructure studied by solid-state MAS NMR

The evolution of the nanostructure upon leaching was followed by MAS NMR. Fig. 15 shows the ^{29}Si MAS NMR spectra for the unleached pastes and after leaching for various times: Fig. 15(a) is for 1Y-WP30, (b) is for 13Y-WP30, and (c) for 13Y-WP50. The sharp peak at around −71.3 ppm on the spectra for the unleached pastes is due to unreacted belite [40], and a small broad peak at around −73.5 ppm is assigned to
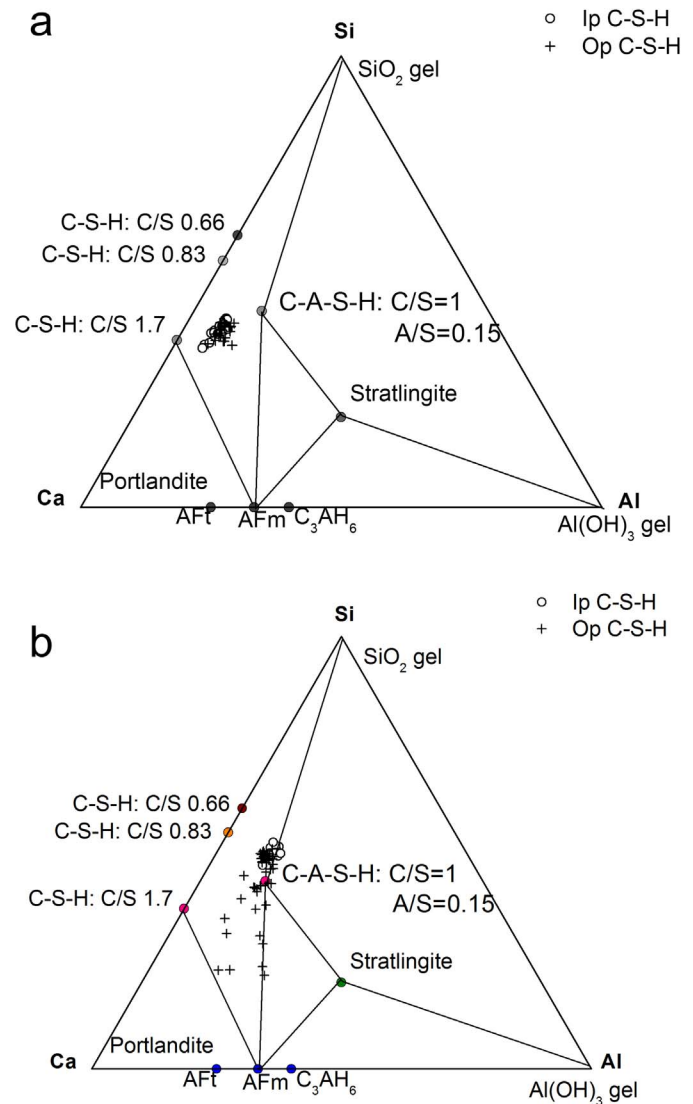
hydrated monomer, Q^0(H) [41]. In addition, two of the eleven spectra appear to have a small, sharper peak superimposed on the Q^0(H), which has been assigned previously for similar pastes to γ-C$_2$S [37,40]. Three main peaks are assigned to the C-A-S-H, i.e. Q^1 (end chain groups or dimer), Q^2 (chain middle groups), and Q^2(1Al) (chain middle groups with one neighbouring Si substituted by Al), which are at approximately −79 ppm, −80.7 ppm and −81.5 ppm, respectively [42–44]. Finally, the broad peak at −103 ppm is due to the glassy pfa [29]. In all cases, the spectrum for the paste after 15 days of leaching is similar to that for the unleached cement paste, except that the intensity of the belite Q^0 peak has decreased as a result of secondary hydration. Whilst the central part of the cement disks used for NMR analysis would have been unaffected by the leaching (as demonstrated on Fig. 9(b)), the close similarity of the spectra for the 15-day and unleached samples suggests that the aluminosilicate anion structure of the C-A-S-H present in the leached parts was also unchanged despite the fact that the Ca/Si ratio was much reduced, from 1.37 to 1.04 at the depth sampled in 13Y-WP30, Table 3. This indicates that it is possible to remove much interlayer Ca without disturbing the aluminosilicate structure. This scenario is modelled on Fig. 16, which shows TEM-EDX data for outer product C-A-S-H free of intermixture with other phases plotted as mean Al/Ca atom ratio against Si/Ca ratio; the error bars correspond to ± 1 standard deviation. The figure includes data for the C-A-S-H in
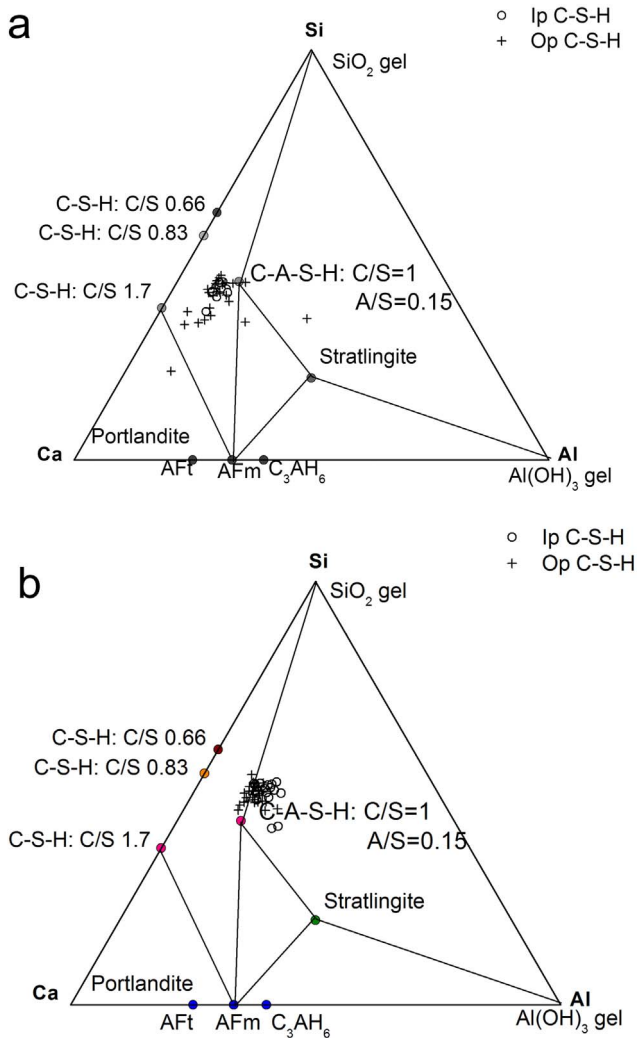
Fig. 14. CaO-Al$_2$O$_3$-SiO$_2$ ternary diagrams for TEM-EDX phase analysis of the C-A-S-H in the 13Y-WP50 cement paste before leaching (a) and after 55 days of leaching (b).

unleached Pc-pfa systems (filled circles), reported previously in Fig. 10 of [13]. The dashed line and the equation are the result of the linear regression analysis of those data. Richardson et al. [13] noted that this linear relationship is essentially the same as determined previously for the C-A-S-H present in ggbs-based systems [45], thus suggesting strongly that it is a compositional relationship that is universal for C-A-S-H that is present in cement blends that incorporate aluminosilicate-rich supplementary cementitious materials. The data for the leached 13Y-30 samples are represented by unfilled squares, the labels indicating the number of days that they were submerged in water. As expected, the data point for the unleached blend is close to the regression line, as is the point for the 5-day sample, consistent with the effects of leaching at that age not having penetrated to the depth sampled by TEM. The data points for the 10- and 15-day leached samples are close to the thick grey line, which shows the effect of progressively removing Ca from the unleached sample with no change in Al or Si i.e. without lengthening of the aluminosilicate anions. The thick black line also corresponds to removal of Ca, but from the 15-day sample instead of the unleached sample, and with the simultaneous addition of Si and Al (in the ratio Si:Al = 2.22) i.e. polymerization of the aluminosilicate chains. It is evident that this simple modelling supports the view that initial removal of Ca from the C-A-S-H does not affect the aluminosilicate structure, lengthening of the chains occurring only when the Ca/Si ratio is reduced to below about 1.

After 45 days of leaching, the spectra on Fig. 15 for all three cement

systems have changed significantly and are similar to one another, indicating a dramatic lengthening of the aluminosilicate in all cases, which is associated with a further reduction in Ca/Si ratio of the C-A-S-H (from 1.04 to 0.85 at the depth sampled in 13Y-WP30, Table 3). Further leaching resulted in the appearance of two extra peaks, i.e. Q^3(1Al) and Q^3, although they are not sufficiently well resolved to decide whether they are due to cross-linking of chains in the C-A-S-H, or alternatively due to the formation of a hydrated alumino-silica gel. If the former, their appearance has been considered previously to be a result of the loss of Ca ions from the interlayer of the C-A-S-H with the formation of hydroxyl groups and then crosslinking [46,47]. The intensity of Q^0 on Fig. 15(a) is much reduced on the spectrum for 45 days of leaching and is absent on the one for 75 days, indicating that the wPc was fully hydrated, which is consistent with the XRD and SEM results. Unfortunately, it is difficult to quantitatively evaluate the relative amounts of each Q^n species due to the complex overlap between the peaks, which is partially due to the range of environments present in poorly ordered C-A-S-H and the consequent chemical shift dispersion [48], and partially due to the inhomogeneous chemical compositions of the C-A-S-H inherent in the leached samples.

Fig. 17(a) shows the ^{27}Al NMR spectra for the unleached 1Y-WP30 cement paste and after 75 days of leaching. The spectrum for the unleached paste has five peaks with maxima at ≈ 69 ppm, ≈ 35 ppm, ≈ 13.3 ppm, ≈ 9.9 ppm and ≈ 4.5 ppm. The peak at ≈ 69 ppm probably has contributions from Al present in the unreacted pfa [49] and Q^2 bridging tetrahedra of aluminosilicate chains of the C-A-S-H; the peak at ≈ 35 ppm has been assigned to Al^{3+} ions present in the interlayer of the C-A-S-H structure substituting for Ca^{2+} ions [50,51]. The resonances at ≈ 13.3 ppm and ≈ 9.9 ppm are due to octahedrally coordinated Al in the AFt and AFm phases respectively [51]. Andersen et al. [52] tentatively ascribed the resonance at ≈ 4.5 ppm to a poorly ordered aluminate hydroxide or calcium aluminate hydrate, produced as a nanostructured surface precipitate on the C-S-H or as separate phase, which they called the *third aluminate hydrate* (TAH) (because it is formed in addition to AFt and AFm), whilst Sun et al. [44] considered that it occurs in the C-A-S-H interlayer (and perhaps on particle surfaces) - together with Al$^{[5]}$ - charge-balancing Al$^{[4]}$ at Q^2 bridging sites through Al$^{[4]}$–O–Al$^{[5,6]}$ linkages. There are two readily observed peaks in the spectrum for the 1Y-WP30 cement paste after 75 days of leaching: a very broad Al$^{[4]}$ peak centred at ≈ 58 ppm, and a second, narrower Al$^{[6]}$ peak at ≈ 9.9 ppm, which is presumably due to some residual AFm, the AFt and TAH having been removed entirely upon prolonged leaching. A resonance at ≈ 58 ppm has been assigned previously to the Al$^{[4]}$ in Q^3 sites in C-A-S-H [44,46,53], although the breadth of the peak in this case suggests that there are multiple contributions e.g. from unreacted pfa, Al at Q^2 bridging sites in C-A-S-H, and possibly also from a hydrated alumino-silica gel. The Al$^{[5]}$ peak observed on the spectrum for the unleached paste (assigned to Al^{3+} substituting for interlayer Ca^{2+} ions in the C-A-S-H [54]) is absent at 75 days, consistent with the removal of interlayer Ca^{2+} ions upon leaching [44]. The Al$^{[6]}$ peak ascribed to TAH is also absent.

Fig. 17(b) shows the ^{27}Al NMR spectra for the unleached 13Y–WP30 cement paste and after 45 days of leaching. Comparison of the spectrum for the unleached paste with that of the unleached 1Y-WP30 cement paste (Fig. 17(a) bottom) indicates that the amount of AFt is reduced relative to the AFm (and TAH), which is consistent with the conversion of AFt to AFm upon additional reaction of aluminate or ferrite after the depletion of calcium sulfate. The spectrum for the paste at 9 years old that is given in Fig. 2 of [13] appears to be at an intermediate stage, thus indicating that changes in the aluminates continued between 9 and 13 years. There are no peaks for Al$^{[5]}$ or TAH on the spectrum for the paste after 45 days of leaching, thus revealing that they are more readily removed upon leaching than either AFm or AFt, perhaps supporting Sun et al.'s [44] view that both peaks are associated with Al in the interlayer or on particle surfaces of C-A-S-H.

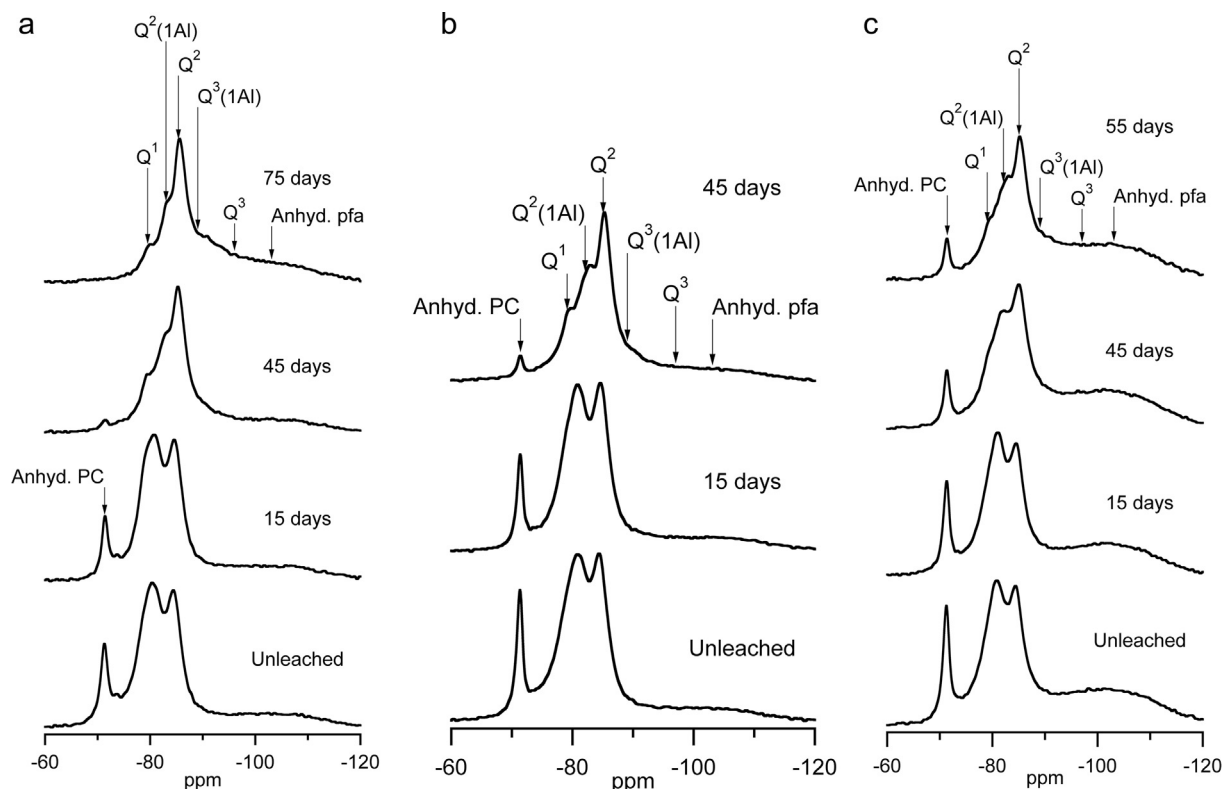Fig. 17(c) shows the ^{27}Al NMR spectra for the unleached 13Y-WP50

Fig. 15. ^{29}Si solid state MAS NMR spectra for the (a) 1Y-WP30, (b) 13Y-WP30 and (c) 13Y-WP50 cement pastes before leaching and at various leaching time.
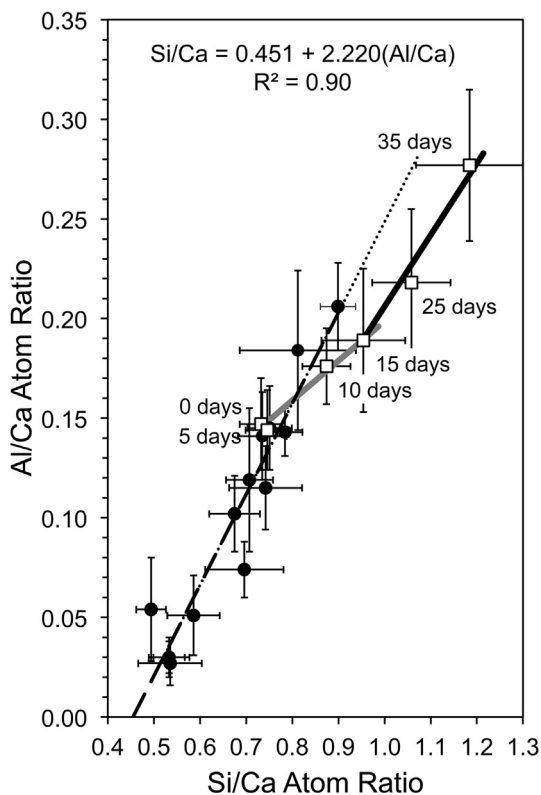

Fig. 16. TEM-EDX data for outer product C-A-S-H free of intermixture with other phases plotted as mean Al/Ca atom ratio against Si/Ca ratio; the error bars correspond to ± 1 standard deviation. The figure includes data for the C-A-S-H in unleached PC-pfa systems (filled circles), reported previously in Fig. 10 of [13], and the data for the leached 13Y-30 sample (unfilled squares), the labels indicating the number of days that the samples were submerged in water for the leaching experiments. The lines are explained in the text.

cement paste and after 55 days of leaching. The spectrum for the unleached paste is similar to those for the 1Y-WP30 and 13Y-WP30 pastes, with the same peak assignments but differing relative intensities. As with the paste with 30% pfa, the spectrum for the unleached 13Y-WP50 paste appears to be a progression from the spectrum at 9 years old (that is given in Fig. 2 of [13]), again indicating that changes in the aluminates continued between 9 and 13 years. Leaching again resulted in complete removal of the peaks assigned to Al[5] and TAH, and to a reduction in the relative intensities of those assigned to AFt and AFm relative to the broad Al[4] peak.

4. Summary and conclusions

Results are reported on the micro- and nano-structural effects of progressively leaching (in deionized water) thin slices (600 μm) of white Portland cement-low calcium pulverized fuel ash (pfa) blended cement pastes containing 30 or 50% pfa. The paste with 50% pfa was aged 13 years prior to leaching and those with 30% pfa were aged 1 and 13 years. Pastes were leached for up to 75 days. The gradual leaching of calcium from the surface of the disks resulted in five microstructural zones, which correspond to the following features:

Zone 0: Unleached.

Zone 1: A reduced quantity of $Ca(OH)_2$ but the C-A-S-H is unaffected.

Zone 2: No large crystals of $Ca(OH)_2$ and the C-A-S-H is unaffected; the microstructure of the cement paste is more porous.

Zone 3: No $Ca(OH)_2$ and the C-A-S-H has a lower Ca/Si ratio than in the unleached paste; the aluminosilicate structure is unaffected until the Ca/Si is reduced to ≈ 1.0 and further reduction is associated with lengthening of the chains. In the 1-year-old pastes studied, the Ca/Si ratio measured by SEM-EDX reduced linearly with distance from zone 2, reducing from the unleached value of 1.43 by $\approx 0.3/100$ μm.

Zone 4: No $Ca(OH)_2$ and the Ca/Si ratio of the C-A-S-H reduced to about 0.6; this zone is only present after significant leaching.

With reference to these five zones, the following useful descriptive
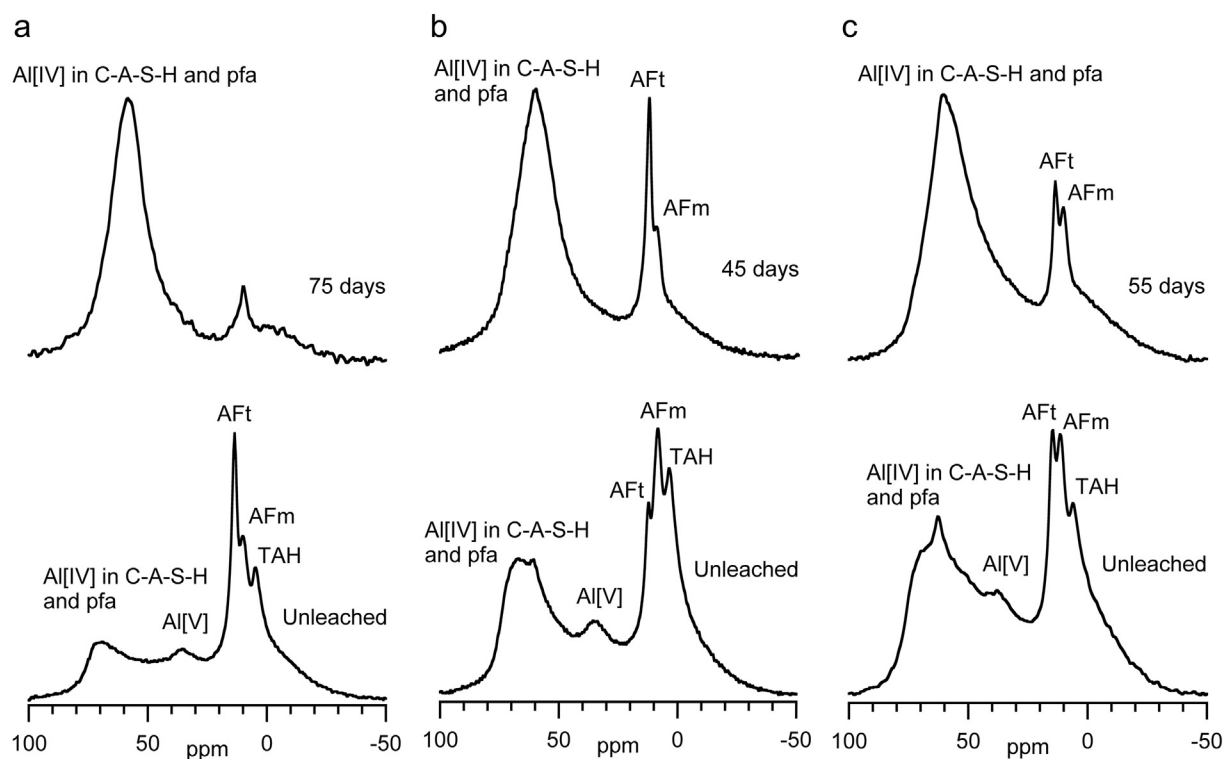
Fig. 17. ^{27}Al solid state MAS NMR spectra for the (a) 1Y-WP30, (b) 13Y-WP30 and (c) 13Y-WP50 cement pastes before leaching and after leaching.

terms can be defined as:

(i) The '*degraded layer*' comprises zones 1 to 4 i.e. it is the part of a sample where there is evidence of microstructural alteration due to leaching;

(ii) the '*CH dissolution depth*' comprises zones 2 to 4 i.e. it is the distance into a sample where there are no longer any large crystals of $Ca(OH)_2$ present (i.e. crystals that are sufficiently large to be resolved by BSE imaging); and

(iii) the '*C-A-S-H decalcification depth*' corresponds to zones 3 and 4 i.e. it is the distance into a sample where a detectable quantity of calcium has been removed from the C-A-S-H.

^{27}Al NMR data showed that Al[5] and TAH were more readily removed upon leaching than either AFm or AFt, perhaps supporting Sun et al.'s [44] view that both are associated with Al in the interlayer or on particle surfaces of C-A-S-H.

Acknowledgements

References

[1] F.P. Glasser, Progress in the immobilization of radioactive wastes in cement, Cem. Concr. Res. 22 (1992) 201–216.

[2] M. Atkins, F. Glasser, Application of Portland cement-based materials to radioactive waste immobilization, Waste Manag. 12 (1992) 105–131.

[3] F. Glasser, M. Atkins, Cements in radioactive waste disposal, MRS Bull. 19 (1994) 33–38.

[4] Serco, Cement Materials for Use as Backfill, Sealing and Structural Materials in Geological Disposal Concepts, SERCO/005125/001Issue (2012), p. 3.

[5] P. Faucon, F. Adenot, J.F. Jacquinot, J.C. Petit, R. Cabrillac, M. Jorda, Long-term behaviour of cement pastes used for nuclear waste disposal: review of physico-chemical mechanisms of water degradation, Cem. Concr. Res. 28 (1998) 847–857.

[6] J. Sharp, J. Hill, N. Milestone, E. Miller, Cementitious systems for encapsulation of intermediate level waste, ASME 2003 9th International Conference on Radioactive Waste Management and Environmental Remediation, Am. Soc. Mech. Eng. (2003) 1425–1433.

[7] Nuclear Decommissiong Authority, Near-field evolution status report, NDA Report NDA/RWMD/033, 2010.

[8] C.R. Wilding, The performance of cement based systems, Cem. Concr. Res. 22 (1992) 299–310.

[9] J.R. Barnes, A.D.H. Clague, N.J. Clayden, C.M. Dobson, C.J. Hayes, G.W. Groves, S.A. Rodger, Hydration of Portland-cement followed by Si-29 solid-state NMR-spectroscopy, J. Mater. Sci. Lett. 4 (1985) 1293–1295.

[10] E. Barry, Beneficiated Fly Ash: Hydration, Microstructure, and Strength Development in Portland Cement Systems, 114 ACI Special Publication, 1989.

[11] K. De Weerdt, M.B. Haha, G. Le Saout, K.O. Kjellsen, H. Justnes, B. Lothenbach, Hydration mechanisms of ternary Portland cements containing limestone powder and fly ash, Cem. Concr. Res. 41 (2011) 279–291.

[12] F. Deschner, F. Winnefeld, B. Lothenbach, S. Seufert, P. Schwesig, S. Dittrich, F. Goetz-Neunhoeffer, J. Neubauer, Hydration of Portland cement with high replacement by siliceous fly ash, Cem. Concr. Res. 42 (2012) 1389–1400.

[13] I.G. Richardson, A.V. Girão, R. Taylor, S. Jia, Hydration of water- and alkali-activated white Portland cement pastes and blends with low-calcium pulverized fuel ash, Cem. Concr. Res. 83 (2016) 1–18.

[14] A. Haworth, S. Sharland, C. Tweed, Modelling of the degradation of cement in a nuclear waste repository, Mater. Res. Soc. Symp. Proc. 127 (1989) 447–454.

[15] F. Adenot, M. Buil, Modelling of the corrosion of the cement paste by deionized water, Cem. Concr. Res. 22 (1992) 489–496.

[16] C. Carde, R. François, J.-M. Torrenti, Leaching of both calcium hydroxide and C-S-H from cement paste: modeling the mechanical behavior, Cem. Concr. Res. 26 (1996) 1257–1268.

[17] D.E. Macphee, K. Luke, F.P. Glasser, E.E. Lachowski, Solubility and aging of calcium silicate hydrates in alkaline solutions at 25 °C, J. Am. Ceram. Soc. 72 (1989) 646–654.

[18] M. Gougar, B. Scheetz, D. Roy, Ettringite and C-S-H Portland cement phases for waste ion immobilization: a review, Waste Manag. 16 (1996) 295–303.

[19] D. Sugiyama, T. Fujita, A thermodynamic model of dissolution and precipitation of calcium silicate hydrates, Cem. Concr. Res. 36 (2006) 227–237.

[20] B.K. Marsh, R.L. Day, Pozzolanic and cementitious reactions of fly ash in blended cement pastes, Cem. Concr. Res. 18 (1988) 301–310.

[21] I.G. Richardson, Electron microscopy of cement, in: P. Barnes, J. Bensted (Eds.), Structure and Performance of Cements, 2nd Edition, E & FN Spon, 2002, pp. 500–556.

[22] S. Gomes, M. François, Characterization of mullite in silicoaluminous fly ash by XRD, TEM, and ^{29}Si MAS NMR, Cem. Concr. Res. 30 (2000) 175–181.

[23] A. Fernandez-Jimenez, A. Palomo, Characterisation of fly ashes. Potential reactivity as alkaline cements, Fuel 82 (2003) 2259–2265.

[24] M.D. Andersen, H.J. Jakobsen, J. Skibsted, Characterization of white Portland

cement hydration and the C-S-H structure in the presence of sodium aluminate by ^{27}Al and ^{29}Si MAS NMR spectroscopy, Cem. Concr. Res. 34 (2004) 857–868.

[25] E. Sakai, S. Miyahara, S. Ohsawa, S.H. Lee, M. Daimon, Hydration of fly ash cement, Cem. Concr. Res. 35 (2005) 1135–1140.

[26] R.S. Gollop, H.F.W. Taylor, Microstructural and microanalytical studies of sulfate attack. II. Sulfate-resisting Portland cement: ferrite composition and hydration chemistry, Cem. Concr. Res. 24 (1994) 1347–1358.

[27] J. Duchesne, E.J. Reardon, Measurement and prediction of portlandite solubility in alkali solutions, Cem. Concr. Res. 25 (1995) 1043–1053.

[28] K. Haga, M. Shibata, M. Hironaga, S. Tanaka, S. Nagasaki, Change in pore structure and composition of hardened cement paste during the process of dissolution, Cem. Concr. Res. 35 (2005) 943–950.

[29] A.V. Girão, The Nanostructure and Degradation of C-S-H in Portland and Blended Cements, School of Civil Engineering, Leeds University, Leeds, 2007.

[30] C.A. Love, Mictrostructure and Silicate Anion Structure of Hardened Blended Cement Pastes, School of Civil Engineering, Leeds University, 2002.

[31] K. Wang, D.C. Jansen, S.P. Shah, A.F. Karr, Permeability study of cracked concrete, Cem. Concr. Res. 27 (1997) 381–393.

[32] R. Taylor, Characterization of C-S-H in Early and Late Age Systems Containing Admixtures, School of Civil Engineering, Leeds University, 2010.

[33] A.W. Harris, M.C. Manning, W.M. Tearle, C.J. Tweed, Testing of models of the dissolution of cements - leaching of synthetic CSH gels, Cem. Concr. Res. 32 (2002) 731–746.

[34] P. Feng, C. Miao, J.W. Bullard, A model of phase stability, microstructure and properties during leaching of portland cement binders, Cem. Concr. Compos. 49 (2014) 9–19.

[35] K. Haga, M. Shibata, M. Hironaga, S. Tanaka, S. Nagasaki, Silicate anion structural change in calcium silicate hydrate gel on dissolution of hydrated cement, J. Nucl. Sci. Technol. 39 (2002) 540–547.

[36] I.G. Richardson, G.W. Groves, The microstructure and microanalysis of hardened ordinary Portland cement pastes, J. Mater. Sci. 28 (1993) 265–277.

[37] A.V. Girao, I.G. Richardson, C.B. Porteneuve, R.M.D. Brydson, Composition, morphology and nanostructure of C-S-H in white Portland cement pastes hydrated at 55 °C, Cem. Concr. Res. 37 (2007) 1571–1582.

[38] I.G. Richardson, The nature of C-S-H in hardened cements, Cem. Concr. Res. 29 (1999) 1131–1147.

[39] S. Diamond, On the glass present in low-calcium and in high-calcium flyashes, Cem. Concr. Res. 13 (1983) 459–464.

[40] A.V. Girão, I.G. Richardson, C.B. Porteneuve, R.M.D. Brydson, Composition, morphology and nanostructure of C–S–H in white Portland cement–fly ash blends

hydrated at 85 °C, Adv. Appl. Ceram. 106 (2007) 283–293.

[41] A.R. Brough, C.M. Dobson, I.G. Richardson, G.W. Groves, In-situ solid-state NMR-studies of Ca3SiO5-hydration at room-temperature and at elevated-temperatures using Si-29 enrichment, J. Mater. Sci. 29 (1994) 3926–3940.

[42] E. Lippmaa, M. Mägi, M. Tarmak, W. Wieker, A.R. Grimmer, A high resolution ^{29}Si NMR study of the hydration of tricalcium silicate, Cem. Concr. Res. 12 (1982) 597–602.

[43] I.G. Richardson, A.R. Brough, R. Brydson, G.W. Groves, C.M. Dobson, Location of aluminum in substituted calcium silicate hydrate (C-S-H) gels as determined by ^{29}Si and ^{27}Al NMR and EELS, J. Am. Ceram. Soc. 76 (1993) 2285–2288.

[44] G.K. Sun, J.F. Young, R.J. Kirkpatrick, The role of Al in C-S-H: NMR, XRD, and compositional results for precipitated samples, Cem. Concr. Res. 36 (2006) 18–29.

[45] I.G. Richardson, G.W. Groves, The structure of the calcium silicate hydrate phases present in hardened pastes of white Portland cement/blast-furnace slag blends, J. Mater. Sci. 32 (1997) 4793–4802.

[46] S. Komarneni, R. Roy, D.M. Roy, C.A. Fyfe, G.J. Kennedy, A.A. Bothnerby, J. Dadok, A.S. Chesnick, Al-27 and Si-29 magic angle spinning nuclear magnetic resonance spectroscopy of Al-substituted tobermorites, J. Mater. Sci. 20 (1985) 4209–4214.

[47] X. Cong, R.J. Kirkpatrick, ^{29}Si MAS NMR study of the structure of calcium silicate hydrate, Adv. Cem. Based Mater. 3 (1996) 144–156.

[48] S.-D. Wang, K.L. Scrivener, ^{29}Si and ^{27}Al NMR study of alkali-activated slag, Cem. Concr. Res. 33 (2003) 769–774.

[49] F. Puertas, A. Fernandez-Jimenez, Mineralogical and microstructural characterisation of alkali-activated fly ash/slag pastes, Cem. Concr. Compos. 25 (2003) 287–292.

[50] M.D. Andersen, H.J. Jakobsen, J. Skibsted, A new aluminium-hydrate species in hydrated Portland cements characterized by ^{27}Al and ^{29}Si MAS NMR spectroscopy, Cem. Concr. Res. 36 (2006) 3–17.

[51] J. Skibsted, C. Hall, Characterization of cement minerals, cements and their reaction products at the atomic and nano scale, Cem. Concr. Res. 38 (2008) 205–225.

[52] M.D. Andersen, H.J. Jakobsen, J. Skibsted, Incorporation of aluminum in the calcium silicate hydrate (C-S-H) of hydrated Portland cements: a high-field Al-27 and Si-29 MAS NMR investigation, Inorg. Chem. 42 (2003) 2280–2287.

[53] J.R. Houston, R.S. Maxwell, S.A. Carroll, Transformation of meta-stable calcium silicate hydrates to tobermorite: reaction kinetics and molecular structure from XRD and NMR spectroscopy, Geochem. Trans. 10 (2009) 1.

[54] P. Faucon, A. Delagrave, J.C. Petit, C. Richet, J.M. Marchand, H. Zanni, Aluminum incorporation in calcium silicate hydrates (C-S-H) depending on their Ca/Si ratio, J. Phys. Chem. B 103 (1999) 7796–7802.